Gaussian Pulse Generators for Subbanded Ultra-Wideband Transmitters

David D. Wentzloff, *Member, IEEE*, and Anantha P. Chandrakasan, *Fellow, IEEE*

***Abstract*—This paper presents calculations for approximating the measured spectrum of pulsed signals in the high and low pulse-repetition-frequency (PRF) region. Experimentally verified peak and average power calculations are presented for pulse trains with no modulation and when modulated by random data using binary phase-shift keying (BPSK). A pulse generator is presented that is built using commercially available discrete components. BPSK pulses are generated at a PRF of 50 MHz. The output spectrum has a center frequency of 5.355 GHz and a −10-dB bandwidth of 550 MHz. A technique for pulse shaping is presented that approximates a Gaussian pulse by exploiting the exponential behavior of a bipolar junction transistor. This technique is demonstrated by a pulse generator fabricated in a 0.18-μm SiGe BiCMOS process. BPSK pulses are generated by inverting a local oscillator signal as opposed to the reference pulse, improving matching. Pulses are transmitted at a PRF of 100 MHz and centered in 528-MHz-wide channels equally spaced within the 3.1–10.6-GHz ultra-wideband band. Measurement results for both transmitters match well with calculated values.**

***Index Terms*—Gaussian, pulse analysis, pulse generation, transmitter, ultra-wideband (UWB).**

I. Introduction

ULTRA-WIDEBAND (UWB) communication is being revisited by the integrated circuits community as a medium for a high data-rate last-meter wireless link. In 2002, the Federal Communications Commission (FCC) allowed UWB communication in the 3.1–10.6-GHz band [1]–[3]. This has triggered a large amount of interest in this area due to the promise of unprecedented wireless data rates and precise positioning in a low-cost consumer radio.

A. FCC Regulations

The FCC restrictions for the UWB band that affect most high data-rate communication systems are the average emissions mask with a maximum of −41.3-dBm/MHz between 3.1–10.6 GHz and the minimum signal bandwidth requirement of 500 MHz within this band. The bandwidth of a UWB signal is defined as the difference between frequencies where the signal power is 10 dB below its maximum level. More of a factor for low pulse-repetition-frequency (PRF) transmitters, the peak power limit set by the FCC is $20\log(\mathrm{RBW}/50)$ dBm, where RBW is the spectrum analyzer resolution bandwidth in megahertz.

Manuscript received August 30, 2005; revised January 14, 2006. This work was supported by the National Science Foundation under Grant ANI-0335256 and by the Hewlett-Packard–Massachusetts Institute of Technology Alliance.

The authors are with the Massachusetts Institute of Technology, Cambridge, MA 02139 USA (e-mail: ddw@mit.edu; anantha@mtl.mit.edu).

Digital Object Identifier 10.1109/TMTT.2006.872053

B. Pulse Modulation Schemes

Several pulse-based modulation schemes are found in literature such as pulse amplitude modulation (PAM), on–off keying (OOK), pulse-position (PPM) or bit-position modulation (BPM), binary phase-shift keying (BPSK), and transmitted reference [4]. BPSK has an advantage over pulse amplitude and position modulation due to an inherent 3-dB increase in separation between constellation points. In a study of UWB single-input single-output (SISO) and multiple-input multiple-output (MIMO) systems employing direct-sequence (DS) BPSK, time-hopping (TH) BPSK, and TH-PPM, the two BPSK systems always outperformed the TH-PPM system. In the single-user case, TH-BPSK and DS-BPSK showed similar performance, while in the multiuser case DS-BPSK outperformed both time-hopping schemes [5].

C. Prior Work

Pulse-based transmitter architectures can be broadly grouped into two categories defining how the pulse energy is generated in the 3.1–10.6-GHz UWB band.

1) The first category includes transmitters that generate a pulse at baseband and up-convert it to a center frequency in the UWB band by mixing with a local oscillator (LO) [6], [7]. The transmitter may not have an explicit mixer that performs the up-conversion mixing. This architecture is easiest identified by having an LO at the center frequency of the pulse. The transmitters characterized in this paper fall into this category.
2) The second category includes transmitters that generate a pulse that directly falls in the UWB band without requiring frequency translation. The pulsewidth for these types of transmitters is usually defined by delay elements that may be tunable or fixed, as opposed to oscillators. A baseband impulse may excite a filter that shapes the pulse [8], [9], or the pulse may be directly synthesized at RF with no additional filtering required [10], [11].

The up-conversion architecture generally offers more diversity and control over the frequency spectrum, but at the cost of higher power since an LO must operate at the pulse center frequency. This architecture is usually found in high data-rate DS communication systems, where the pulse shape and center frequency must be well defined [6], [7].

For most transmitters, the radiated frequency spectrum is defined by the shape of the pulse. Approximations to a Gaussian pulse shape and its derivatives are common due to their favorable time and frequency response. The analog approach to a Gaussian pulse generator is to use translinear and exponential

0018-9480/$20.00 © 2006 IEEE

circuits to perform mathematical operations in the analog domain that result in a Gaussian shape [12], [13]. Derivatives of a Gaussian pulse may be generated with a second-order bandpass filter acting as a differentiator. Other approaches approximate a Gaussian pulse by shaping with a bank of gm-C filters [8] or by switching a reactive load and using the transient response for shaping [9]–[11].

A $\pi/2$-shift BPSK transmitter has been reported that synthesizes baseband pulses by summing weighted currents at a sample rate of 4 GS/s. The I and Q pulse trains are then up-converted to a 4-GHz center frequency [6]. A sinusoidal monocycle pulse generator has been reported that generates pulses by gating an LO on for one complete period of the LO frequency. Thus, the spectrum of the transmitted pulse is centered on this frequency. This transmitter supports both BPSK and PPM modulation schemes at a PRF of 1.625 GHz [7].

II. Pulsed-UWB Measurements

The measurement procedure for pulsed-UWB signals varies from that for narrowband signals. There are two distinct regions in which the measurement results obtained with a spectrum analyzer (SA) follow different trends for peak and average measurements of modulated and repetitive (unmodulated) pulse trains. These two regions are defined by the ratio of the SA resolution bandwidth (RBW) to the PRF. One must be conscious of this ratio in order to correctly interpret measured results. This section presents a tutorial on calculations for approximating spectral measurements of pulsed signals with an SA [14], [15]. The expressions given are for peak and average power levels measured at the center frequency of the pulse, assuming that this is the maximum value. These calculations are used to analyze measured results from the pulse generators in Sections IV and V. The SA used for all measurements is an Agilent 8564EC.

A. Pulse Desensitization Correction Factor

For narrow pulses defined by a pulsewidth PW $< 0.1/$RBW, the IF filter of the SA cannot completely respond to the pulse. In this case, the SA measures the pulsed response of its IF filter, rather than the pulse itself. Thus, a pulse desensitization correction factor (PDCF) is defined to relate the peak power measured by an SA to the actual peak power of the pulse [14]. There are several restrictions described in [14] on the setup of the SA to ensure accurate results when applying the PDCF.

The PDCF depends on the shape of the pulse. In order to accommodate arbitrary pulse shapes, the envelope of the RF pulse can be approximated by a rectangular pulse with the same peak voltage and area as the arbitrary pulse shape. The effective width τ_{eff} of the rectangular pulse is calculated by

$$\tau_{\text{eff}} = \int_0^{\frac{1}{\text{PRF}}} \frac{p(t)dt}{V_{\text{pk}}} \tag{1}$$

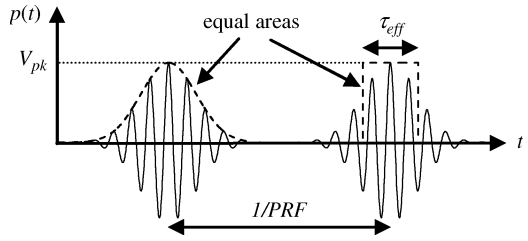

Fig. 1. Definitions for pulse and equivalent rectangular pulse of width τ_{eff}.

where $p(t)$ is an arbitrary pulse shape and V_{pk} is the peak voltage of the pulse as shown in Fig. 1 [14]. The measured peak power of a pulse train without modulation is related to V_{pk} by

$$P_{\text{pk}}^{no\ \text{mod}} = 10\log\left(\frac{V_{\text{pk}}^2}{Z_0}\right) + \text{PDCF}. \tag{2}$$

The PDCF is defined for the *low-* and *high-PRF* regions in Section II-C, and Z_0 is the characteristic impedance.

B. Modulated Power Calculation

The average power of a pulse train modulated by a random sequence of data can also be calculated from the actual peak power of a pulse. The derivation can be readily found in communication textbooks, therefore only the result is repeated here. The power spectral density for a 1-Ω load in W/Hz is given by

$$G(f) = \text{PRF} \cdot |P(f)|^2 \tag{3}$$

where $P(f)$ is the Fourier transform of the pulse voltage waveform. For the rectangular pulse with effective pulsewidth τ_{eff}, the average power spectral density of a modulated pulse train is calculated by

$$P_{\text{avg}}^{\text{mod}} = 10\log\left(\frac{V_{\text{pk}}^2}{Z_0}\right) + 20\log(\tau_{\text{eff}}) + 10\log(\text{PRF} \cdot \text{RBW}). \tag{4}$$

In a study conducted on several UWB transmitters [15], it was reported that a measurement using an SA with an rms average detector provides the most accurate average power reading. The rms detector is more robust to the UWB signaling schemes than the logarithmic average typically used for narrowband average power measurements. In one case of pulsed measurements, the logarithmic average under-reported the rms average power by 10–15 dB.

C. Measurement Trends in Low-/High-PRF Regions

The measurement of peak and average power for modulated and repetitive pulse trains can be divided into two regions. These are defined by the ratio of RBW to PRF being greater or less than 1. This section summarizes the measurements in these two regions. At the transition region around where PRF = RBW, the measured spectrum is highly dependent on the modulation and SA filter response and is therefore more difficult to predict [15].

1) Low-PRF Region ($RBW/PRF > 1.7$): In this region, pulses are spaced far enough apart in time to allow the output of the IF filter in the SA to return to zero between each pulse. Because of this, the peak and average measurements are *independent* of whether modulation by random data is applied or not, therefore $P_{\mathrm{pk}}^{\mathrm{mod}} = P_{\mathrm{pk}}^{no\ \mathrm{mod}}$ and $P_{\mathrm{avg}}^{\mathrm{mod}} = P_{\mathrm{avg}}^{no\ \mathrm{mod}}$. Average power is calculated from (4).

The peak power in the *low*-PRF region (modulated or unmodulated) measured by the SA can be approximated by (2), where

$$\mathrm{PDCF} = 20\log(\tau_{\mathrm{eff}} \cdot \mathrm{RBW} \cdot k_{\mathrm{pulse}}) \tag{5}$$

and k_{pulse} relates the RBW frequency to an effective IF bandwidth for pulsed signals [14]. The value of k_{pulse} depends on the SA used and varies from 1.5 to 1.617. The peak power measurement is independent of PRF and has a $20\log(\ )$ dependence on RBW and τ_{eff}.

2) High-PRF Region ($RBW/PRF < 0.3$): In this region, the RBW is sufficiently narrow such that a "line spectrum" of impulses spaced at the PRF is visible on the SA for a repetitive pulse train of identical pulses. Peak and average power measurements are effected by modulation in this region. The average power of a repetitive pulse train is equal to the peak power, $P_{\mathrm{avg}}^{no\ \mathrm{mod}} = P_{\mathrm{pk}}^{no\ \mathrm{mod}}$. The unmodulated peak (and average) power measured by the SA can be approximated by (2), where

$$\mathrm{PDCF} = 20\log(\tau_{\mathrm{eff}} \cdot \mathrm{PRF}). \tag{6}$$

$P_{\mathrm{pk}}^{no\ \mathrm{mod}}$ has a $20\log(\ )$ dependence on PRF and τ_{eff}, and is independent of RBW.

For modulated signals that are similar to Gaussian noise, the measured average power is given by (4). The measured peak power will be 7–11 dB above the average power level, statistically depending on the amount of time the peak measurement is taken over [15]. Both peak and average power of modulated signals follow a $10\log(\ )$ dependence on RBW and PRF in the high-PRF region.

D. Experimental Verification

To illustrate the measurement trends for each region, various measurements were performed on a rectangular pulse train. BPSK modulated pulses were generated with an arbitrary waveform generator and up-converted to a 5-GHz center frequency. An instantaneous peak pulse amplitude of 50.8 mV was measured with an oscilloscope. The pulsewidth was 50 ns, which is equal to τ_{eff} since the pulse is rectangular. The RBW was varied from 10 kHz to 2 MHz, and the PRF varied from 100 kHz to 2 MHz. Plots of the measurements spanning the *low*- and *high*-PRF regions are shown in Fig. 2.

Peak power was measured with the SA positive peak detector, a video bandwidth (VBW) of 3 MHz, and a sweep time of 1 s. The measurements for modulated and unmodulated peak power matched very well with the predicted values and followed the predicted trends for varying PRF and RBW in their respective regions.

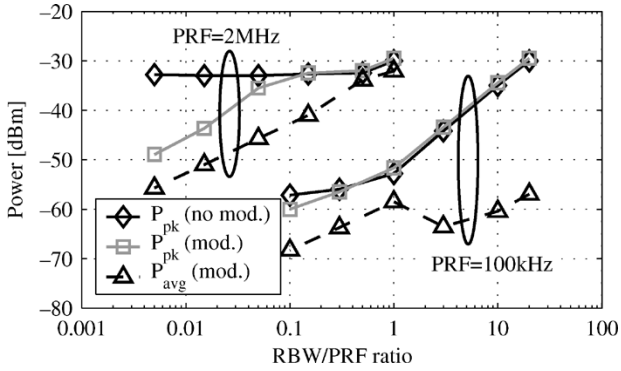

Fig. 2. Measurements of a rectangular pulse up-converted to 5 GHz with $\tau_{\mathrm{eff}} = 50$ ns and PRF $= 100$ kHz and 2 MHz. For each measurement, RBW is swept from 10 kHz to 2 MHz.

Average power was measured with the SA detector in sample mode, a VBW of 3 MHz, and the sweep time set to auto. An rms detector was not available for these measurements. The noise marker featured on the SA was used to measure the average power of the modulated signal, which is similar to Gaussian noise. This marker displays the logarithmic average of trace points around a selected frequency, and corrects for errors due to averaging and a wider effective RBW [16]. The results matched with calculations except for the RBW/PRF > 1 region, where the power was under-reported by up to 12 dB. These results are similar to those found in [15], where the logarithmic average was found to under-report the average power by 10–15 dB for low duty-cycle impulsive signals. An rms detector was reported not to suffer from this problem. Average power follows the expected $10\log(\mathrm{PRF} \cdot \mathrm{RBW})$ trend in both regions.

III. System Architecture

The following sections presents two pulse generators designed for a custom UWB transceiver. This architecture uses pulse-based BPSK modulation, where information is encoded as a pulse with either positive or negative polarity [17]. The maximum PRF supported is 100 MHz. Data are represented with 31 pulses per bit during the packet preamble and one pulse per bit during the packet payload. The maximum data rate is therefore 100 Mb/s. The baseband pulse train is up-converted to one of 14 evenly spaced, 528-MHz-wide channels in the 3.1–10.6-GHz UWB band. This frequency plan has been adopted from an 802.15.3a proposal, with the exception that fast frequency hopping is not implemented [18]. A block diagram of the architecture is shown in Fig. 3.

The receiver performs I/Q direct conversion to baseband, where the received signal is sampled by dual 5-b 500-MS/s analog-to-digital converters (ADCs). Coarse acquisition, channel estimation, fine tracking, and demodulation are all performed in the digital baseband. A mostly digital architecture was chosen for greater flexibility, however, performing correlations in the analog domain can result in lower power [19]. Amplitude and timing matching between transmitted positive and negative BPSK pulses are critical to the quality of service. Mismatch between pulses affects the coarse acquisition and demodulation algorithms. The linearity requirement in the

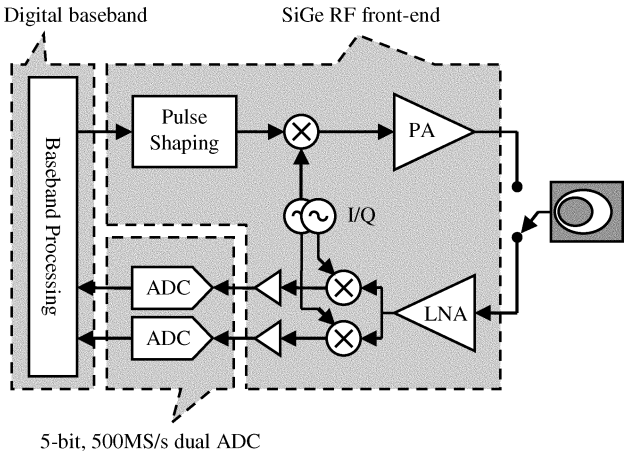

Fig. 3. 100-Mb/s 14-channel UWB system architecture.

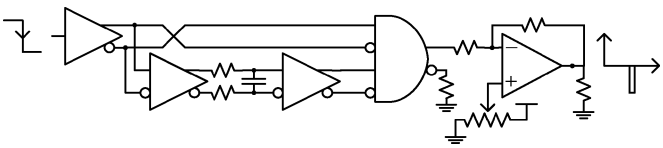

Fig. 4. ECL pulse generator and level shifter for the discrete pulse generator. On every falling edge of the input clock, a negative pulse is generated with an effective width of $\tau_{\text{eff}} = 2.4$ ns.

transmitter is relaxed since the receiver records the pulse shape before demodulation.

IV. Discrete Pulse Generator

A transmitter has been built using commercial off-the-shelf discrete components as part of a complete prototype transceiver [20]. It is designed for BPSK modulation of pulses at a variable PRF of up to 50 MHz. Pulses are up-converted to a center frequency of 5.355 GHz. The maximum data rate supported is 50 Mb/s. Individual packets are downloaded from a PC to the transmitter in real time over a USB interface.

A. Hardware Description

The architecture of the transmitter is similar to the custom chipset architecture shown in Fig. 3. Baseband pulses are generated by the circuit shown in Fig. 4. A transistor–transistor logic (TTL)-level clock operating at the PRF is converted to 3.3-V emitter-coupled logic (ECL) levels. The inverted clock and a delayed clock are inputs to an AND gate, the output of which is a pulse on every falling edge of the input clock. The pulsewidth is set by an *RC* filter between two ECL buffers. The output of the ECL AND gate is at 1.6–2.4-V levels; therefore, a high-speed inverting level shifter is used to bring the pulse down to 0 V.

The baseband pulses are then modulated and up-converted to a center frequency of 5.355 GHz using the circuit shown in Fig. 5. Depending on the data bit, the pulse is switched to either the positive or negative input of a differentiating amplifier using high-frequency analog switches. When each switch is in the OFF position, it terminates the input of the amplifier to ground. Both switches are turned off to put the transmitter in an idle state outputting no pulses. This state can also be used to vary the PRF. The output of the amplifier is a BPSK modulated pulse train

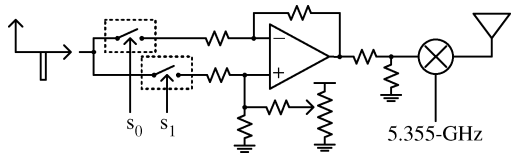

Fig. 5. Schematic of the modulation and up-conversion circuit for the discrete pulse generator.

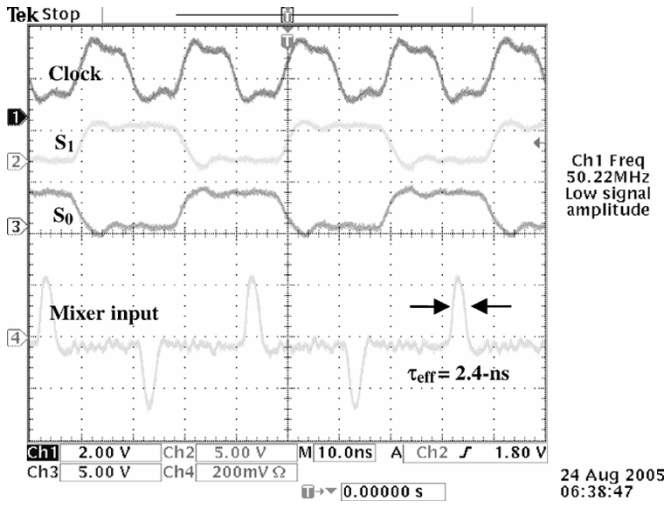

Fig. 6. Plot of the input clock and switch signals for the discrete pulse generator at a PRF of 50 MHz. The pulses are sampled at the input to the up-conversion mixer.

which is attenuated and up-converted to 5.355 GHz by a passive mixer. An offset adjustment is provided at the positive input of the amplifier to correct for offsets at the input of the mixer. This adjustment is necessary to minimize LO feedthrough to the antenna.

B. Experimental Results

A screen capture of the discrete pulse generator in operation is shown in Fig. 6. The top trace is the input clock of 50 MHz, and the two traces beneath the clock are the switch input signals S_0 and S_1. The bottom trace is the pulse train measured at the input to the mixer and after the attenuator. This pulse train is subsequently up-converted to a 5.355-GHz center frequency.

The spectrum of the pulses has a -10-dB bandwidth of 550 MHz. The effective rectangular pulsewidth τ_{eff} is 2.4 ns, which is calculated from the frequency of the first null in the measured spectrum by $\tau_{\text{eff}} \approx 1/(f_{1\text{st null}} - f_{\text{center}})$. The peak voltage of the up-converted pulse is 104 mV. These measured values were used in the equations from Section II to calculate peak and average power levels, which are compared to the spectrum measurements in Table I. The peak and average modulated measurements were taken with the transmitter outputting 250 kb of pseudorandom data. Measurements were made at 50-MHz and 50-kHz PRF to demonstrate the accuracy of the calculations in the *low*- and *high*-PRF regions.

V. Integrated Tanh Pulse Generator

A transmitter has been fabricated in a 0.18-μm SiGe BiCMOS process as part of the custom chipset for a 100-Mb/s pulse-based UWB transceiver discussed in Section III [21],

TABLE I
DISCRETE TRANSMITTER MEASUREMENT RESULTS

		Measured	Calculated
High-PRF Region	Un-modulated P_{pk}	-25.9-dBm	-25.2-dBm
PRF=50-MHz	Modulated P_{avg}	-43.4-dBm	-42.2-dBm
RBW/PRF=0.02	Modulated P_{pk}	-32.2-dBm	-31.2-dBm
Low-PRF Region	Un-modulated P_{pk}	-54.1-dBm	-55.0-dBm
PRF=50-kHz	Modulated P_{avg}	-73.8-dBm	-72.2-dBm
RBW/PRF=20	Modulated P_{pk}	-53.5-dBm	-55.0-dBm

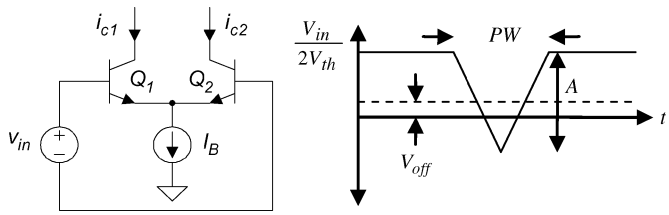

Fig. 7. BJT differential pair and input voltage waveform for generating a tanh pulse.

[22]. The transceiver architecture is shown in Fig. 3. The goal of this work was to design a low-power UWB transmitter that emits Gaussian-shaped pulses due to their desirable time and frequency response. By exploiting the exponential behavior of a BJT, the Gaussian pulse can be accurately approximated with an elegant analog circuit that simultaneously performs up-conversion mixing to the 3.1–10.6-GHz band. Pulses are up-converted to one of 14 channel center frequencies. The center frequencies are set by

$$f_{\text{center}} = 2904 + 528 \cdot n_{\text{ch}}[\text{MHz}] \tag{7}$$

where $n_{\text{ch}} = 1, 2, \ldots, 14$.

A. Tanh Pulse Shaping

The transmitter uses a differential pair of BJTs with a triangle signal input to generate and shape a pulse of one polarity, which is shown conceptually in Fig. 7. For the proper choice of A, PW, and V_{off}, the current i_{C2} will have a shape that approximates that of a Gaussian.

For a fixed bias current I_B, the collector currents in the differential pair are approximately related by

$$I_B = i_{C1} + i_{C2}. \tag{8}$$

By substituting terms into the exponential equations for collector current of a BJT, it can be shown using hyperbolic identities that the collector current i_{C2} is described by

$$i_{c2} = \frac{1}{2} I_B \left[1 - \tanh\left(\frac{V_{\text{in}}}{2V_{\text{th}}} \right) \right] \tag{9}$$

where V_{th} is the thermal voltage, equal to kT/q.

The output current i_{C2} of the differential pair will be a pulse with tanh-shaped rising and falling edges for the triangle input signal shown in Fig. 7. Note that the y axis is normalized to $V_{\text{in}}/2V_{\text{th}}$, which is the argument of the tanh function in (9). Current i_{C1} is not used and can be terminated to the power supply.

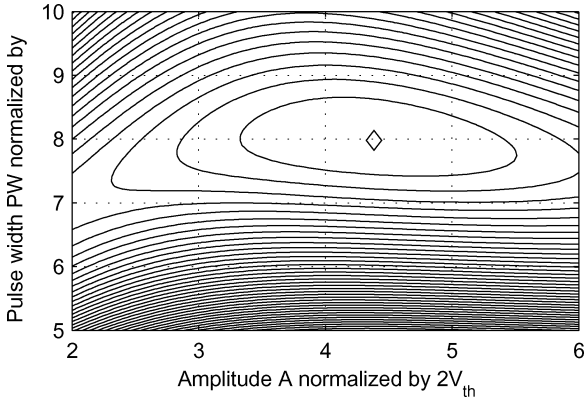

Fig. 8. Mean squared error contours and minimum error point for $\sigma = 1.0$, $V_{\text{off}} = 1.0$.

The pulse is simultaneously up-converted to the UWB band by additionally modulating the tail current I_B with an LO. Furthermore, BPSK pulses are generated by inverting the LO signal in the tail current.

This architecture has several benefits, which are: 1) the input signal begins and ends at the same level; thus, there is no "reset" phase required as in differentiating pulse generators, eliminating transients; 2) positive and negative pulses can be generated with the same triangle input signal and inverted LO to improve matching, which is difficult to achieve with complementary circuits; 3) up-conversion is performed by adding an LO signal to the tail current I_B and, thus, no additional mixer is required; and 4) the triangle signal can be generated with well-known techniques, and the accuracy of the Gaussian approximation is not sensitive to small deviations in the values of A and PW.

B. Optimization

The optimal values for A, PW, and V_{off} were found by sweeping each variable and searching for the minimum mean-squared error (MSE) between the resulting tanh-shaped pulse and the Gaussian pulse given by

$$V_{\text{Gauss}} = V_p e^{-\frac{t^2}{2\sigma^2}}. \tag{10}$$

The energies of the two pulses are equalized before calculating the MSE. A contour plot of the MSE is shown in Fig. 8 for $V_{\text{off}} = 1.0$ and $\sigma = 1.0$. The diamond indicates the values of A and PW, resulting in the minimum MSE. A plot of the corresponding tanh-shaped pulse for the minimum MSE point is compared with a Gaussian reference pulse in Fig. 9. The time- and frequency-domain responses are shown. The side lobes of the tanh-shaped pulse are 45 dBr. The results of the parameter optimization are as follows.

1) Normalized Amplitude A: The amplitude normalized to $2V_{\text{th}}$ does not vary with σ and varies linearly with V_{off} for $V_{\text{off}} > 1.0$. The equation for setting A is

$$A = 2.4 + 2.0 \cdot V_{\text{off}}. \tag{11}$$

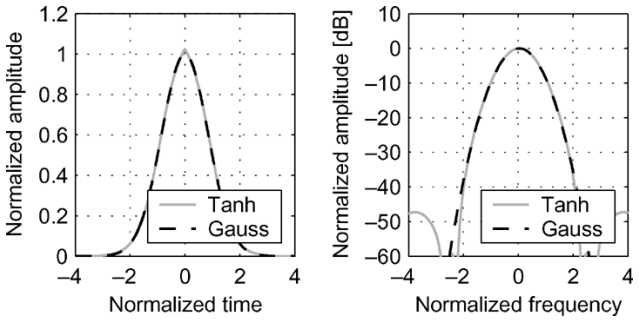

Fig. 9. Time and frequency response of the optimized tanh pulse for $\sigma = 1$ and $V_{\rm off} = 1.0$.

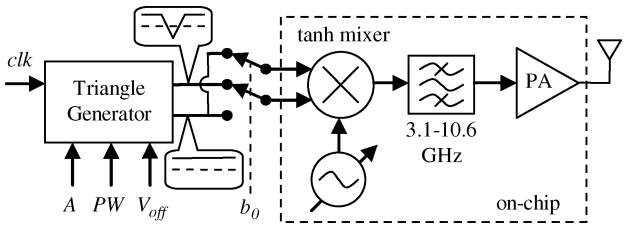

Fig. 10. BPSK UWB transmitter block diagram.

2) Pulsewidth PW: The pulsewidth is proportional to σ and varies linearly with $V_{\rm off}$ for $V_{\rm off} > 1.0$. The equation for setting PW is

$$\mathrm{PW} = \sigma(4.37 + 3.61 \cdot V_{\rm off}). \tag{12}$$

3) Normalized Offset $V_{\rm off}$: The offset normalized to $2V_{\rm th}$ does not vary with σ and should be greater than 1.0 for best results. Making it arbitrarily large does not improve the response, and it should remain within the biasing constraints of the circuit

$$V_{\rm off} \geq 1.0. \tag{13}$$

As shown in Fig. 8, the minimum MSE between the tanh and Gaussian pulses is broad. This relaxes the requirements on the circuitry used to generate the triangle signal. It also relaxes the dependency of the pulse shape on temperature through $V_{\rm th}$. Varying temperature over a range of 0 °C–85 °C (28% of Kelvin) results in an 11% variation in bandwidth and 0.2 dB in peak power for the pulse shown in Fig. 9.

C. Transmitter Architecture

A block diagram of the transmitter is shown in Fig. 10. The triangle signal is implemented off-chip but is suitable for integration. To generate BPSK pulses, the triangle signal is switched to either the positive or negative input of the mixer. The inactive mixer input is simultaneously switched to a constant voltage. The same triangle signal is used to generate both polarity pulses to improve matching between pulses. The triangle signal switch also has an off state to implement variable PRF or a standby mode. The up-converted pulse is filtered and amplified on-chip before being dc-coupled to the off-chip UWB antenna.

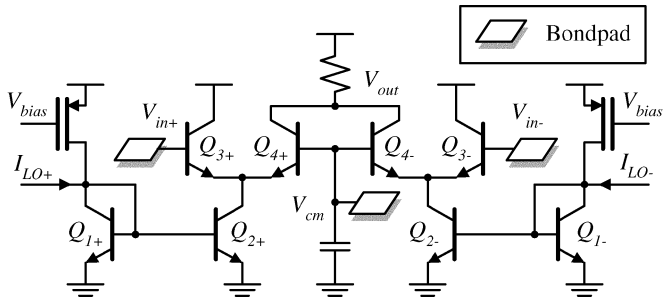

Fig. 11. Schematic of the tanh pulse-shaping UWB mixer.

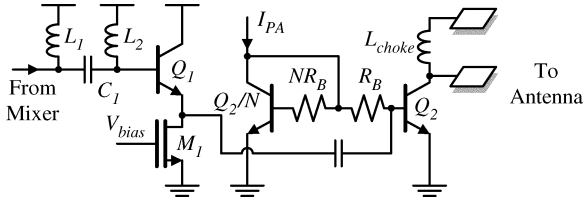

Fig. 12. Schematic 3.1–10.6-GHz filter and PA.

D. Circuit Description

A schematic of the tanh pulse-shaping mixer is shown in Fig. 11. At the core are two tanh-shaping pulse generators made by transistors $Q_{3+/-}$ and $Q_{4+/-}$. The tail currents of the pulse generators are modulated by LO signals. This enables simultaneous pulse shaping and up-conversion mixing. The LO signals to the two pulse generators are 180° out of phase, giving the inversion for BPSK pulse generation.

The LO signal is generated on-chip or can be switched to an external source and can be tuned from 3.1 to 10.6 GHz. The LO signal path is balanced to ensure equal amplitudes and 180° phase difference between the differential signals. The differential LO signals are converted to a current and mirrored, along with a bias current, into the tails of the two differential pairs.

Up-converted positive or negative pulses are generated by applying the triangle input signal to $V_{\rm in+}$ or $V_{\rm in-}$, respectively. The triangle signal voltage is relative to $V_{\rm cm}$, which is at a fixed potential. Applying the triangle signal to $Q_{3+/-}$ with the bases of $Q_{4+/-}$ fixed reduces unwanted signals from coupling to the output. The output currents of the differential pairs are summed at node $V_{\rm out}$. This provides first-order cancellation of LO feedthrough, similar to a double-balanced Gilbert cell mixer.

A schematic of the UWB band select filter and power amplifier (PA) is shown in Fig. 12. The mixer output is fed into the filter made by L_1, L_2, and C_1, providing a second-order roll-off below 3 GHz to reduce out-of-band emissions. The simulated frequency response of the mixer and filter is plotted in Fig. 13. The signal is then buffered and ac-coupled to the PA. The PA is class A, with an RF choke at the output, and can be dc-coupled to the antenna.

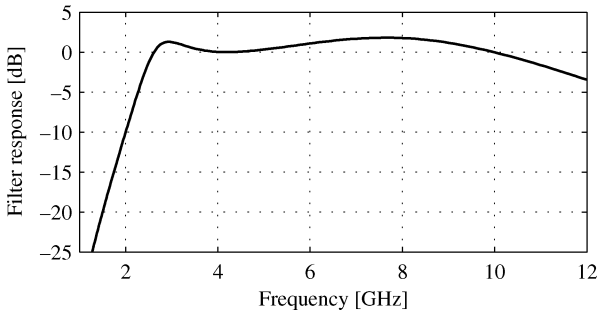

Fig. 13. Simulated ac response of the LO path through the mixer and filter.

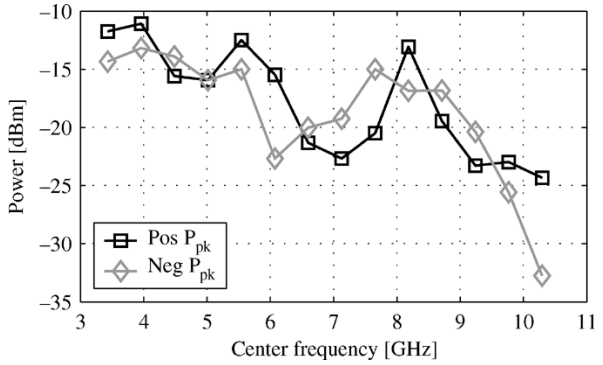

Fig. 14. Unmodulated peak power matching between positive and negative pulses.

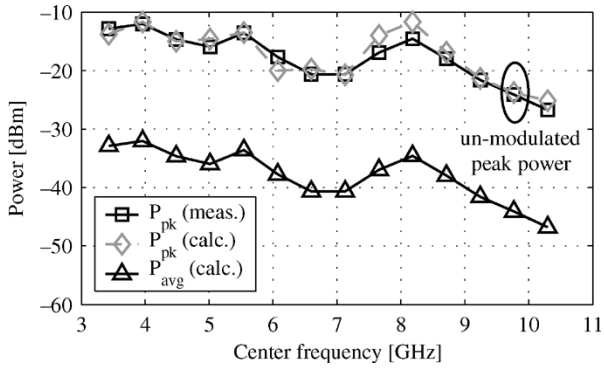

Fig. 15. Plot of the pulse power levels in the 14 UWB channels. Peak power reported is with no modulation. Modulated peak power is expected to be 11 dB above modulated average power.

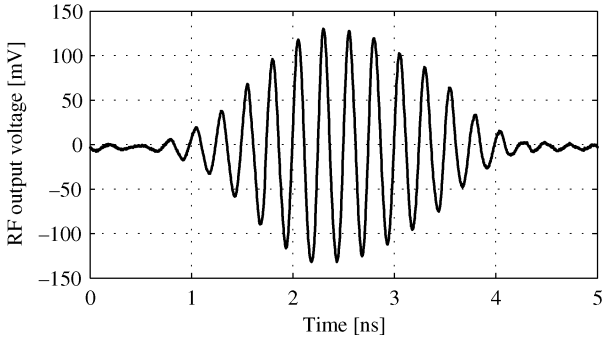

Fig. 16. Measured pulse modulated by a 4.0-GHz external LO.

E. Experimental Results

The transmitter was fabricated in a 0.18-μm SiGe BiCMOS process, and packaged in a 48-lead MLF/QFN package which is a wire-bonded package. Due to a resonance with the bondwires at the input of the mixer, the pulses generated in channels 6–10 were distorted and did not have a Gaussian shape. An external LO was used as the center frequency of the pulses for all measurement results.

The matching between positive and negative pulses was evaluated at each of the center frequencies by measuring the peak power and bandwidth of a train of all positive or all negative pulses. An external LO was used to set the center frequency of the pulses, with an on-chip, single-to-differential converter to generate the differential LO used for inverting pulses. This converter has inherent mismatch in its differential outputs that varies with frequency, which can directly lead to mismatch between positive and negative pulse amplitudes. The spectral measurements fall into the *high*-PRF region for a PRF of 100 MHz and RBW of 1 MHz; therefore, a line spectrum is observed for a repetitive pulse train and peak power levels are independent of RBW. The measurements of peak pulse power in each channel are shown in Fig. 14. The undistorted pulse responses demonstrated matching better than 2.5 dB.

The peak voltage V_p of the RF pulse envelope was measured at each center frequency with a high-speed sampling oscilloscope. The effective pulsewidth was approximated from the spectrum measurement by $\tau_{\text{eff}} \approx 1(f_{1\text{st null}} - f_{\text{center}})$. This was used in (2) and (6) to predict the measured peak power level. The calculated and measured results can be compared in Fig. 15.

TABLE II
TRANSMITTER SPECIFICATIONS SUMMARY

V_{DD}	1.8-V
Mixer and LO buffering power	25.2-mW
PA power	6.1-mW
Total power	31.3-mW
Pulse repetition frequency	100-MHz
Modulation	BPSK
Effective pulse width τ_{eff} (ch. 1-5, 11-14)*	1.7-3.3-ns
-10-dB bandwidth** (ch. 1-5, 11-14)*	426-558-MHz

*Pulses in channels 6-10 distorted by resonance at mixer input
**Weighted average BW of positive and negative pulses in each channel

Each peak power data point is the rms average of the negative and positive pulse powers at that center frequency. There is very good agreement between the calculated and measured peak powers. This peak power is of an unmodulated pulse train.

The average power of a pulse train modulated with random data is calculated using (4) with measured data and plotted in Fig. 15. This data is based on an rms average of the positive and negative pulse peak power levels. The -41.3-dBm/MHz FCC limit is exceeded in some channels using nominal biasing; however, this can be corrected by reducing the gain adjustment in the power amplifier. The modulated peak power is expected to be 11 dB above the average power and follows a $10\log(\text{RBW})$ trend in the high-PRF region [5]. For a 2-MHz RBW, the calculated peak power does not exceed the FCC limit of -28 dBm when the -41.3-dBm/MHz average power limit is not exceeded.

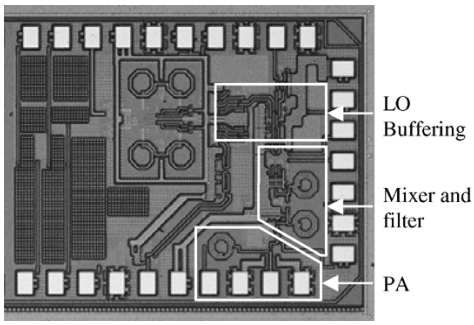

Fig. 17. Die photograph of the transmitter with a tanh-shaping pulse generator. The dimensions are 1.7 mm × 1.4 mm.

A measured pulse with a center frequency of 4 GHz is shown in Fig. 16 as an example of an up-converted tanh-shaped pulse. Table II provides a summary of the pulse generator specifications. A die photograph of the transmitter is shown in Fig. 17.

VI. Conclusion

The measurement results from a spectrum analyzer for peak and average power of modulated and unmodulated pulse trains depends on the ratio of RBW to PRF. For typical high data-rate transmitters, RBW/PRF $\ll 1$, and therefore peak and average power of a modulated pulse train have a $10\log(\,)$ dependence on PRF and RBW. Calculations of peak and average power can be made from the peak voltage and effective pulsewidth. Spectral measurements for a discrete pulse generator and custom integrated pulse generator match well with these calculations.

A transmitter built from discrete components has been presented for use in a UWB prototyping platform. The transmitter communicates with BPSK pulses and a variable PRF up to 50 MHz. Pulses are up-converted to a 550-MHz band centered on 5.355 GHz.

A technique for generating pulses that accurately approximates a Gaussian shape has been presented. By exploiting the exponential properties of a BJT, a near-Gaussian pulse is shaped from a triangle input signal. Pulse shaping is integrated into the mixer, performing up-conversion and shaping in one simple circuit. The tanh pulse generator has been fabricated in a 0.18-μm SiGe BiCMOS process. Pulse shaping is limited in channels 6–10 due to parasitics on the mixer input. Matched BPSK pulses and near-Gaussian pulse generation has been demonstrated at a PRF of 100 MHz in all other channels.

References

[1] FCC, "First report and order," FCC 02-48, Feb. 2002.
[2] FCC, "Order," FCC 05-58, Mar. 2005.
[3] FCC, "Second report and order and second memorandum opinion and order," FCC 04-285, Dec. 2004.
[4] T. Q. S. Quek and M. Z. Win, "Ultrawide bandwidth transmitted-reference signaling," in *Proc. IEEE Int. Commun. Conf.* , Jun. 2004, vol. 6, pp. 3409–3413.
[5] M. Welborn, "System considerations for ultra-wideband wireless networks," in *Proc. IEEE Radio Wireless Conf.*, Aug. 2001, pp. 5–8.
[6] S. Iida *et al.*, "A 3.1 to 5 GHz CMOS DSSS UWB transceiver for WPANs," in *Proc. IEEE Int. Solid-State Circuits Conf.*, Feb. 2005, vol. 48, pp. 214–215.
[7] A. Azakkour, M. Regis, F. Pourchet, and G. Alquie, "A new integrated monocycle generator and transmitter for Ultra-wideband (U Wl3) communications," in *Proc. IEEE Radio Frequency IC Symp.*, Jun. 2005, pp. 79–82.
[8] S. Bagga, W. A. Serdijn, and J. R. Long, "A PPM Gaussian monocycle transmitter for ultra-wideband communication," in *Proc. Int. Ultra Wideband Syst. Technol. Conf.*, May 2004, pp. 130–134.
[9] Y. Jeong, S. Jung, and J. Liu, "A CMOS impulse generator for UWB wireless communication systems," in *Proc. Int. Symp. Circuits Syst.*, May 2004, vol. 4, pp. 129–132.
[10] K. Marsden *et al.*, "Low power CMOS re-programmable pulse generator for UWB systems," in *Proc. Int. Ultra Wideband Syst. Technol. Conf.*, Nov. 2003, pp. 443–447.
[11] H. Kim, D. Park, and Y. Joo, "All-digital low-power CMOS pulse generator for UWB system," *Electron. Lett.*, vol. 40, no. 24, pp. 1534–1535, Nov. 2004.
[12] M. Rodriguez and J. Silva-Martinez, "A fully-programmable temperature-compensated analogue circuit for gaussian functions," in *Proc. IEEE Int. Symp. Circuits Syst.*, May 2000, pp. 481–484.
[13] H. Kim, D. Park, and Y. Joo, "Design of CMOS Scholtz's monocycle pulse generator," in *Proc. IEEE Ultra Wideband Syst. Technol. Conf.*, Nov. 2003, pp. 81–85.
[14] "Spectrum analysis. . . pulsed RF," Agilent Technol., Palo Alto, CA, Applicat. Note 150-2, May 2005.
[15] W. A. Kissick, "The temporal and spectral characteristics of ultrawideband signals," NTIA, U.S. Dept. Commerce, Boulder, CO, NTIA Rep. 01-383, Jan. 2001.
[16] "Spectrum analyzer measurements and noise," Agilent Technol., Palo Alto, CA, Applicat. Note 1303, Feb. 2003.
[17] R. Blazquez *et al.*, "A baseband processor for pulsed ultra-wideband signals," in *Proc. IEEE Custom Integr. Circuits Conf.*, Oct. 2004, pp. 587–590.
[18] "Multiband OFDM physical layer proposal for IEEE 802.15.3a/," MultiBand OFDM Alliance, IEEE P802.15 Working Group for Wireless Personal Area Networks (WPAN's), Sep. 2004.
[19] M. Verhelst *et al.*, "Architectures for low power ultra-wideband radio receivers in the 3.1–5 GHz band for data rates $<$10 Mbps," in *Proc. Int. Low Power Electron. Des. Symp*, Aug. 2004, pp. 280–285.
[20] D. D. Wentzloff *et al.*, "System design considerations for ultra-wideband communication," *IEEE Commun. Mag.*, vol. 43, no. 8, pp. 114–121, Aug. 2005.
[21] R. Blazquez *et al.*, "Direct conversion pulsed UWB transceiver architecture," *Proc. Design, Autom. Test. Eur.*, pp. 94–95, Mar. 2005.
[22] D. D. Wentzloff and A. P. Chandrakasan, "A 3.1–10.6 GHz ultra-wideband pulse-shaping mixer," in *Proc. IEEE Radio Freq. IC Symp.*, Jun. 2005, pp. 83–86.

David D. Wentzloff (M'02) received the B.S.E. degree from The University of Michigan at Ann Arbor, in 2000, the S.M. degree from the Massachusetts Institute of Technology (MIT), Cambridge, in 2002, and is currently working toward the Ph.D. degree in electrical engineering at MIT. His doctoral thesis concerns power electronics and electric machines.

His research interests include RF front-end circuit design for ultra-wideband communication.

Anantha P. Chandrakasan (M'95–SM'01–F'04) received the B.S, M.S., and Ph.D. degrees in electrical engineering and computer sciences from the University of California at Berkeley, in 1989, 1990, and 1994, respectively.

Since September 1994, he has been with the Massachusetts Institute of Technology (MIT), Cambridge, where he is currently the Joseph F. and Nancy P. Keithley Professor of Electrical Engineering. His research interests include low-power digital integrated circuit design, wireless microsensors, UWB radios, and emerging technologies. He coauthored *Low Power Digital CMOS Design* (Kluwer, 1995) and *Digital Integrated Circuits* (Pearson Prentice-Hall, 2003, 2nd ed.). He also coedited *Low Power CMOS Design* (IEEE Press, 1998), *Design of High-Performance Microprocessor Circuits* (IEEE Press, 2000), and *Leakage in Nanometer CMOS Technologies* (Springer-Verlag, 2005).

Dr. Chandrakasan has served as a Technical Program co-chair for the 1997 International Symposium on Low Power Electronics and Design (ISLPED), VLSI Design'98, and the 1998 IEEE Workshop on Signal Processing Systems. He was the Signal Processing Sub-Committee chair for ISSCC 1999–2001, the Pro-

gram vice-chair for ISSCC 2002, the Program chair for ISSCC 2003, and the Technology Directions Sub-Committee chair for ISSCC 2004–2006. He is the Technology Directions chair for ISSCC 2007. He was an Associate Editor for the IEEE JOURNAL OF SOLID-STATE CIRCUITS from 1998 to 2001. He serves on the IEEE Solid State Circuits Society (IEEE SSCS) Administrative Committee (AdCom) and is the Meetings Committee chair. He was the recipient of several awards including the 1993 IEEE Communications Society's Best Tutorial Paper Award, the IEEE Electron Devices Society's 1997 Paul Rappaport Award for the Best Paper in an EDS publication, the 1999 Design Automation Conference Design Contest Award, and the 2004 DAC/ISSCC Student Design Contest Award.